

# HADRONIC SIGNATURES OF DECONFINEMENT IN RELATIVISTIC NUCLEAR COLLISIONS\*

**Jan Rafelski<sup>†</sup>, Jean Letessier and Ahmed Tounsi**

Department of Physics, University of Arizona, Tucson, AZ 85721

Laboratoire de Physique Théorique et Hautes Energies<sup>‡</sup>  
Université Paris 7, 2 place Jussieu, F-75251 Cedex 05.

September 30, 1997

Dedicated to Professor Wieslaw Czyz on occasion of his 70th birthday

## Abstract

We describe the remarkable accomplishments of the current heavy ion Pb–Pb collision experiments involving strange particle production, carried out at 158A GeV at CERN–SPS. These experimental results, together with the earlier 200A GeV S-induced reactions, imply that, at central rapidity, a novel mechanism of strangeness production arises, accompanied by excess entropy formation. We argue that:

- these results are consistent with the formation of a space-time localized, highly excited, dense state of matter;
- the freeze-out properties of strange hadrons are suggestive of the formation of a color-deconfined, thermally and nearly chemically equilibrated phase, which provides at present the only comprehensive framework to describe all experimental data;
- the matter fireball is undergoing a transverse expansion with nearly the velocity of sound of relativistic matter; longitudinal expansion is not in the scaling regime.

We present a first analysis of the recent Pb–Pb results and discuss several alternative reaction scenarios. We evaluate quantitatively strangeness production in the deconfined quark-gluon phase and obtain yields in agreement with the experimental observations made in 200A GeV S–W and 158A GeV Pb–Pb interactions. We also present a qualitative discussion of  $J/\Psi$  results consistent with our understanding of strange particle results.

PACS numbers: 25.75.+ , 12.38.Mh, 24.85.+p

---

\*Presented by Jan Rafelski at XXXVII Cracow School of Theoretical Physics, Zakopane May 30 – June 10, 1997

<sup>†</sup>Support by US-Department of Energy under grant DE-FG03-95ER40937.

<sup>‡</sup>Unité associée au CNRS UA 280.

# 1 Hadronic Probes of QGP

For many years now, we have searched to understand what happens to nuclear matter when it is perturbed by a high energy hadron [1]. Our present day interest originates in the hope and expectation that novel physical phenomena arise in collisions of heaviest nuclei, at center of momentum energy exceeding many times the nuclear rest mass. Specifically, it is believed today that, in such collisions, we compress and significantly excite the nuclear matter of which the nuclei are made, ultimately dissolving the quarks confined in hadrons into a bizarre new liquid [2].

The present day experimental study of dense hadronic matter formed in relativistic nuclear collisions is completely dominated by the intense search for our modern times nuclear Holy Grail, the quark-gluon plasma (QGP). QGP state must exist according to simple interpretation of quantum chromodynamics (QCD), the theory of strong interactions. In short, when temperature exceeds about 150–200 MeV, the structured QCD vacuum melts, individual hadrons dissociate and fuse [3] and a macroscopic space time region, filled with free, movable quarks and gluons is formed.

At low temperature, in the confining vacuum phase, only individual hadronic particles such as  $\pi$ ,  $\rho$ ,  $N$ ,  $\Delta$ , *etc.*, can exist, they are in our cold world the condensation drops of the deconfined state. The great variety of observed hadrons results from the complex nature of the QCD interactions and it indirectly implies that the structure and properties of highly excited hadronic matter could be very diverse.

We will compare the experimental data with reaction models invoking two most opposite states of matter:

- the conventional, confined phase we shall call hadronic gas (HG), made of hadronic particles of different type in local thermal equilibrium, with masses and degeneracies in most cases well known. Along with Hagedorn [4], we subsume that particle–particle strong interactions in HG are accounted for by giving the short lived hadronic resonances the status of independent statistical fractions;
- the ‘melted’ QGP phase consisting of a nearly free gas of quarks and gluons, interacting perturbatively, an approach which is properly justified only in the limit of ultra high energy densities, as seen, *e.g.*, in the framework of finite temperature lattice gauge theory QCD simulations [5].

Since in the collision of large nuclei, the highly dense state is formed for a rather short time of magnitude  $2R/c$ , where  $R$  is the nuclear radius, one of the major challenges has been to identify suitable physical observables of deconfinement. This difficult problem of detecting reliably the formation of an unknown phase of matter, existing only  $0.5 \cdot 10^{-22}$ sec, has not been completely resolved today. The electromagnetic probes involving directly produced photons and dileptons are witnesses to the earliest moments of the reaction, but their production rates are in general very small. Indeed, the direct photon signal remains up to this day undetected, since the experimental  $\gamma$  yield is dominated by the secondary processes  $\pi^0 \rightarrow \gamma + \gamma$ . The dilepton yield is also mostly resulting from meson decays, but there are some kinematic regions where this background yield is very small. Moreover, the dilepton spectrum gives interesting insights about the vector meson yields and their variation with experimental conditions. We will briefly address here this very interesting observable when considering  $J/\Psi$  production in the final section, concentrating instead on directly detected hadronic yields and spectra. In passing we note that aside of spectra of hadronic particle, one can also relatively easily measure particle

correlations. The two particle HBT correlation measurement is widely used to determine the geometric properties of the central fireball [6], and the results agree with a reaction picture between the nuclei relying on geometric considerations.

In this work, we primarily update our comprehensive presentation [7] of strangeness (charm) and entropy as signature of the deconfined phase. Strangeness and entropy are good observables since both will be preserved by ‘reasonable’ evolution scenarios of the dense matter fireball: the melted QGP state is in general entropy richer than the frozen HG phase [8]. Once entropy has been generated, it cannot be lost, an entropy excess accompanies QGP formation. When abundant particle production is possible, this entropy excess is seen as an enhancement in the total hadronic particle multiplicity with each (relativistic) meson carrying about 4 units of entropy out of the interaction region.

Similarly, strangeness is in general more abundant in QGP than HG phase [9], and it is not reannihilated in rapid decomposition of the dense matter state [10]. It has become a key diagnostic tool of dense hadronic matter because:

- 1) particles containing strangeness are produced more abundantly in relativistic nuclear collisions than it could be expected based on simple scaling of  $p$ - $p$  reactions;
- 2) all strange quarks have to be made, while light  $u$ ,  $d$  quarks are also brought into the reaction by the colliding nuclei;
- 3) because there are many different strange particles, we have a very rich field of observables with which it is possible to explore diverse properties of the source;
- 4) theoretical calculations suggest that glue–glue collisions in the QGP provide a sufficiently fast and thus by far, a unique mechanism leading to an explanation of strangeness enhancement.

There are two generic flavor observable (strangeness and charm) which we study analyzing experimental data, and we introduce these here, without an effort to ‘orthogonalize’, *i.e.*, make them independent of each other:

- absolute yield of strangeness/charm  
Once produced in hot and dense hadronic matter, *e.g.*, the QGP phase, strangeness/charm is not reannihilated in the evolution of the deconfined state towards freeze-out, because in the expansion and/or cooling process the rate of production/annihilation rapidly diminishes and becomes negligible. Therefore the flavor yield is characteristic of the initial, most extreme conditions.
- phase space occupancy  $\gamma_i$   
 $\gamma_i$  describes how close the flavor yield per unit of volume ( $i = s, c$ ) comes to the chemical equilibrium expected;  $\gamma_i$  impacts strongly the distribution of flavor among final state hadronic particles.

Because of the high density of the QGP phase, the phase space occupancy  $\gamma_i$  can saturate rapidly, and thus particle abundances will emerge from a chemically equilibrated  $u$ ,  $d$ ,  $s$  phase, which is hardly imaginable for conventional reaction mechanisms. Because entropy and strangeness are enhanced in a similar way in QGP, the specific yield of strangeness per particle produced is not a good quantity to use when searching for the deconfined state. Many other strategies are available, of which we favor measurement of the specific entropy yield per participating baryon, accompanied by a study of relative strange antibaryon yields, involving particle ratios such as  $\bar{\Lambda}/\bar{p}$  [9]. It is remarkable that the pertinent results obtained for S–Pb collisions by the NA35 collaboration [11] have shown the QGP related enhancement.

We use here the framework of local thermal equilibrium, and thus we will now briefly survey the different equilibria possibly present in the nucleus–nucleus high energy collisions. The principal reason to use the statistical description in study of dynamics of dense hadronic matter is that considerable simplicity can result, compared for example with dynamical models involving collisional cascading of individual particles. We realize considerable economy in the description of the physical system by invoking a local thermal equilibrium. When we speak of equilibrium in a rapidly evolving system, such as is the dense, highly excited phase of hadronic matter, we always imply *local* equilibrium: specifically, within the local space-time region the temperature parameter  $T$  describes the energy content of the individual degrees of freedom. Even with this restriction, we cannot generally subsume that statistical description always makes good sense, since it implies presence of many degrees of freedom in mutual interaction. We believe that strongly interacting degrees of freedom involved in collisions of large atomic nuclei will participate in the equipartition of energy through elastic or inelastic collisions, justifying the introduction of local temperature.

Since any local thermal equilibrium will be overlaid by diverse flow phenomena, how can we experimentally see that our hypothesis is indeed consistent with the data? First, we note that spectra of particles produced have, in the transverse mass variable  $m_{\perp} = \sqrt{m^2 + p_{\perp}^2}$ , a ‘thermal’ shape, consistent with a thermal and expanding source. The inverse slope of the  $m_{\perp}$  spectra provides a measure of the temperature, and it can vary from one kind of particle to another due to different freeze-out properties of different particle and mass dependence of flow. What supports strongly the notion of local thermal equilibrium is the experimental fact that, at given  $m_{\perp}$ , very different particles have, in the same reaction,  $m_{\perp}$ -spectra that sport the same inverse slope (temperature). There seems to be presently no exception from this  $m_{\perp}$ -scaling rule, even though widely different ‘temperatures’ are sometimes quoted for different particles; it turns out on closer inspection that the domains of good, precise data points which weight heavily in the spectral fits are in very different ranges of  $m_{\perp}$  where different slopes are reported. It is thus quite difficult to compare different particles in the same  $m_{\perp}$ -range, with the exception of comparing particles with antiparticles, where indeed same spectral shapes are typically seen (see, *e.g.*,  $\bar{\Lambda}$  and  $\Lambda$  spectra). One must be further aware that, even in most central symmetric collisions, a good fraction of colliding nucleons,  $\mathcal{O}(15\%)$ , will not participate in the dynamics of centrally colliding matter, contributing to a longitudinal flow background.

We further recognize two different forms of chemical equilibria. To see the need for this differentiation consider a hot, thermally equilibrated gas of colliding nucleons  $N$ , pions  $\pi$ , and  $\Delta$ -resonances. The relative abundance of the  $u$  and  $d$  carrying quarks is easily established through flavor exchange reactions, such as  $p + \pi^{-} \leftrightarrow n + \pi^0$ , at the quark level there is no creation or annihilation process that need to occur in each reaction to equilibrate the flavors. We speak in such type of reactions of relative chemical equilibration through quark exchange reactions. Very much different is the approach to equilibrium involving the equilibration of the number of mesons and baryons. Baryon-antibaryon formation processes involving heavy mesons, that is of the type  $N + \bar{N} \leftrightarrow \rho + \omega$  require that aside of the reorganization of the quark content, also the number of valance quarks changes. Such processes are typically much slower than those leading to establishment of relative chemical equilibrium, since the inelastic reactions that change the particle abundance have usually much smaller cross section than particle number preserving exchange reaction. While thermal and relative chemical equilibrium will in general occur within the life span of hadronic reaction, approach to absolute chemical equilibrium provides interesting chronometric information about the dynamics of the collision

process.

At the level of elementary QCD degrees of freedom, it is the production of heavy flavors which is the primary off-equilibrium aspect of chemical equilibration. At current SPS energies, where the inverse  $m_{\perp}$ -slopes observed are in the range  $T = 250\text{--}300$  MeV for strange baryons and other heavy particles, the chances for thermal production of charm are not big; however, at RHIC and LHC considerable greater temperatures and possibly longer life span of the dense matter is expected, and thus we can hope and expect that it will become possible to study charm approach to absolute chemical equilibrium.

In the next section we survey the experimental strange particle results obtained in Pb–Pb collisions. This is followed by updates of our work of last years [7]: recent advance in developing more precise understanding of strange and charm flavor production in deconfined phase is presented in section 3; our analysis of the Pb–Pb results is presented in section 4; in the final section we consider the possibility that quark gluon plasma has been discovered in the SPS experiments.

## 2 Strange particles in Pb–Pb reactions

The possibility that strange particle anomalies seen in recent years at SPS in Sulphur induced reactions on heavy nuclei are arising in consequence to the formation of a deconfined QGP phase has stimulated the intense continuation of the experimental research program in the considerably more difficult, high particle multiplicity environment arising in Pb induced reactions, which are presently possible at 158A GeV.

We address [12] several (7 today) available ratios of strange and anti strange baryons measured by the WA97–collaboration [13] and two such ratios measured by the NA49–collaboration [14, 15]. These ratios appear only on first sight to be much like the earlier 200A GeV S–W and S–S data of experiments WA85 and WA94 [16]. The NA49–collaboration has also presented the rapidity and transverse mass spectra of  $\Lambda$ ,  $\bar{\Lambda}$  and kaons [14]; the latter result are consistent with the central transverse mass spectra already reported by the NA44–collaboration [17]. The NA49–collaboration stresses that there is no major change in the yield of strangeness per particle multiplicity, compared to the earlier study of S–S and S–Au interactions [18]; this is in agreement with our expectation that strangeness and entropy (multiplicity) grow at the same rate as we change from S- to Pb-induced reactions, assuming that in both cases QGP/gluon fusion mechanisms (see next section) are at the origin of strangeness production.

First NA49 results about the production of  $\phi = s\bar{s}$  are also already available [19]. The revised inverse slopes of the  $\phi$  are reported at  $T = 280$  MeV, in agreement with temperatures of all heavy ( $m \simeq 1$  GeV) strange particles such as  $\Lambda$ ,  $\bar{\Lambda}$ . The experiment NA49 further reports an important change in the shape of rapidity spectra [14]: the  $\Lambda$ ,  $\bar{\Lambda}$  and kaon rapidity distributions are localized around mid-rapidity and are, in particular in case of  $\Lambda$ , much narrower than previously seen in S-induced reactions, with a rapidity shape corresponding to a radiating, thermal source undergoing transverse and longitudinal expansion. The rapidity spectra of  $\Lambda$ ,  $\bar{\Lambda}$  are presented in Fig. 1; the scaling of the yields (factor 8.5 for  $\Lambda$  and factor 5.5 for  $\bar{\Lambda}$ ) hides somewhat from view the strong concentration in Pb–Pb reactions of the  $\Lambda$  yield at central rapidity.

The WA97–collaboration stresses that an enhancement in the  $\Omega/\Xi$  ratio in Pb–Pb compared

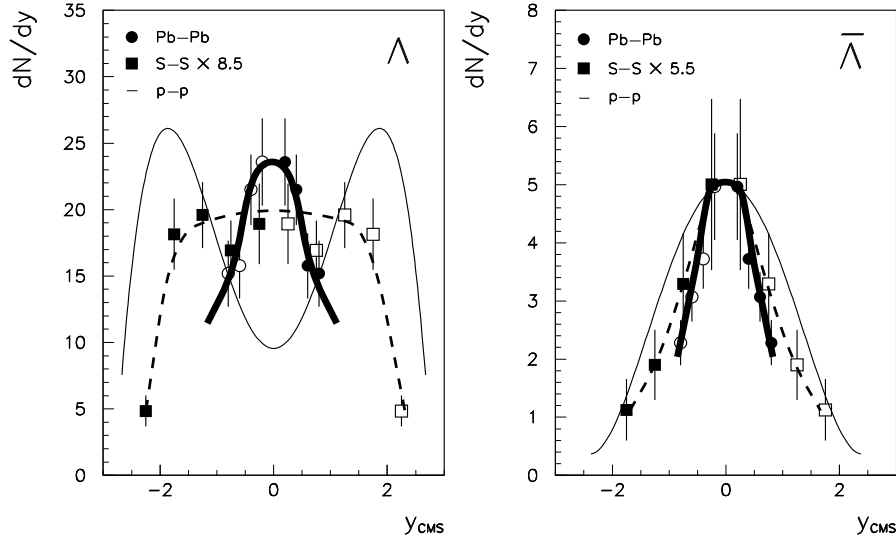


Figure 1: Rapidity distribution of  $\Lambda$  (left hand side) and  $\bar{\Lambda}$  (right hand side). Circles (and thick solid line to guide the eye): Pb–Pb collisions at 158A GeV; squares (and dashed line) scaled S–S collisions at 200A GeV (factor 8.5 for  $\Lambda$  and factor 5.5 for  $\bar{\Lambda}$ ), and thin solid line, shape expected from p–p data. Open symbols: reflection around central rapidity. Data by NA49 collaboration [14])

to p–Pb collisions:

$$\frac{(\Omega + \bar{\Omega})/(\Xi + \bar{\Xi})|_{\text{Pb-Pb}}}{(\Omega + \bar{\Omega})/(\Xi + \bar{\Xi})|_{\text{p-Pb}}} \simeq 3 \quad (> 2, \text{ at } 95\% \text{ C.L.}).$$

The significance of the last result is that hadronic cascades tend to attenuate the yield of multistrange hadrons in strangeness exchange reactions and thus such an enhancement is not natural for a reaction picture involving hadrons-hadrons collisions. This can be thus taken as evidence that direct formation and emission from a hot fireball of deconfined matter is the prevailing mechanism for the production of multistrange baryons and antibaryons.

The experiment WA97 [13] has further reported several specific strange baryon and antibaryon ratios from Pb–Pb collisions at 158A GeV, comprising 30% of inelastic interactions. All ratios are obtained in an overlapping kinematic window corresponding effectively to transverse momentum  $p_{\perp} > 0.7$  GeV, within the central rapidity region  $y \in y_{cm} \pm 0.5$ . They have been corrected for weak interactions cascading decays. The experimental values are:

$$R_{\Lambda} = \frac{\bar{\Lambda}}{\Lambda} = 0.14 \pm 0.03, \quad R_{\Xi} = \frac{\bar{\Xi}}{\Xi} = 0.27 \pm 0.0, \quad R_{\Omega} = \frac{\bar{\Omega}}{\Omega} = 0.42 \pm 0.12, \quad (1)$$

$$R_s^{\text{P}} = \frac{\bar{s}}{\Lambda} = 0.14 \pm 0.02, \quad R_{\bar{s}}^{\text{P}} = \frac{\bar{\Xi}}{\Lambda} = 0.26 \pm 0.05, \quad (2)$$

$$R_s^{\text{P}'} = \frac{\Omega}{\Xi} = 0.19 \pm 0.04, \quad R_{\bar{s}}^{\text{P}'} = \frac{\bar{\Omega}}{\Xi} = 0.30 \pm 0.09. \quad (3)$$

Here, the lower index s, resp.  $\bar{s}$ , reminds us that the ratio measures the density of strange, resp. antistrange, quarks relatively to light quarks. The upper index p indicates that the

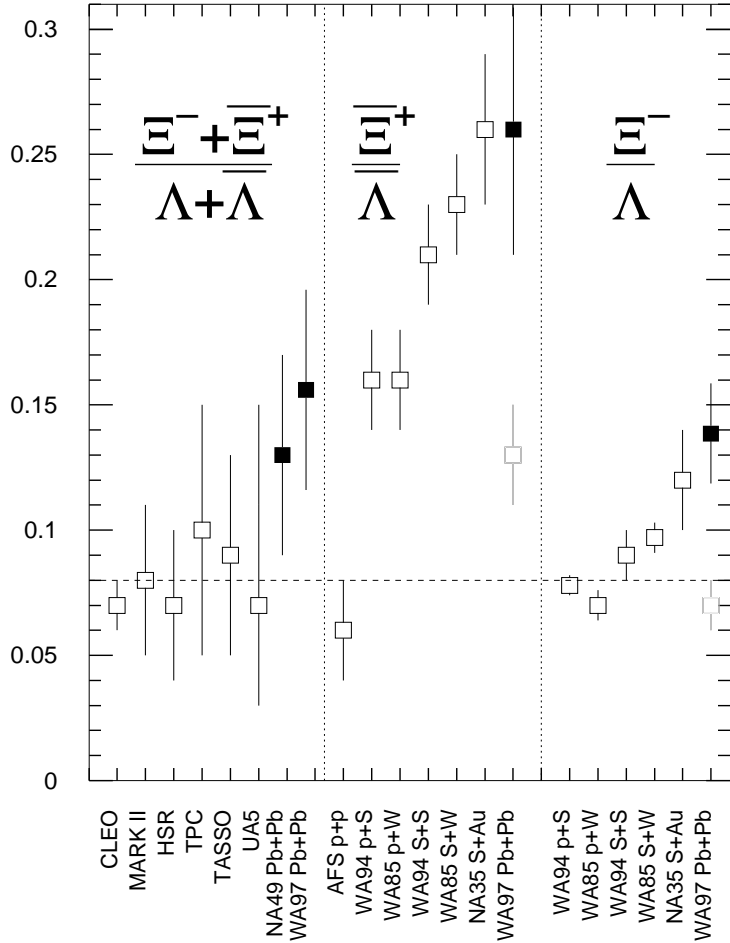


Figure 2: Sample of World results (as ‘function’ of experiment name for yields involving ratio of strange to non-strange quarks in baryons. Dark squares: recent Pb–Pb results.

ratio is taken within a common interval of transverse momenta (and not common transverse mass). We compare  $R_s^p$ ,  $R_s^p$  results with earlier measurements in Fig. 2. The strange antibaryon enhancement effect is reconfirmed in the Pb–Pb data, and we see that there is no major change of this result, which determines the phase space occupancy of strangeness, as we move from S–S or S–W/Pb results to Pb–Pb results.

There is agreement between WA97 and NA49 on the value of  $R_\Lambda$ , even though the data sample of NA49 is taken for more central trigger, constrained to as few as 4% of most central collisions. The cuts in  $p_\perp$  and  $y$  are nearly identical in both experiments. From Fig. 3 in [14], we obtain the value  $R_\Lambda = 0.17 \pm 0.03$ , which we shall combine with the value given by WA97 and we thus take in our data fit:

$$R_\Lambda = \frac{\bar{\Lambda}}{\Lambda} = 0.155 \pm 0.04. \quad (4)$$

We should keep in mind that for seven different particle yields measured only five ratios are independent of each other. The two constraints are:

$$\frac{R_\Xi}{R_\Lambda} = \frac{R_s^p}{R_s^p}, \quad \frac{R_\Omega}{R_\Xi} = \frac{R_s^p}{R_s^p}. \quad (5)$$

Despite this, in our fit to the above data, we shall retain all seven independently determined ratios as presented here and the error  $\xi^2$  will correspond to sum of seven relative square errors.

The experiment NA49 also reported [15]:

$$\frac{\Xi + \bar{\Xi}}{\Lambda + \bar{\Lambda}} = 0.13 \pm 0.03. \quad (6)$$

While this ratio can be expressed in terms of the three other ratios

$$\frac{\Xi + \bar{\Xi}}{\Lambda + \bar{\Lambda}} = R_s \frac{1 + R_\Xi}{1 + R_\Lambda}, \quad (7)$$

it is again a separate measurement which thus can be fitted independently.

We will now estimate the ratio of hyperons to kaons, required in some of our studies below. We note that the NA49 spectra [14] of kaons and hyperons have a slightly overlapping domain of  $m_\perp$ . We recall that the slopes are not exactly equal, thus all we can do is to try to combine the two shapes, assuming continuity consistent with flow, and to estimate the relative normalization of both that would place all experimental points on a common curve. We have carried out this procedure and obtained:

$$\left. \frac{\Lambda}{K_s^0} \right|_{m_\perp} \simeq 6.2 \pm 1.5. \quad (8)$$

Note that there is a tacit presumption in our approach that a similar effective  $\Delta y$  interval was used in both spectra. We recall that this ratio was  $4.5 \pm 0.2$  in the S-W data [20].

We now consider at the experimental inverse  $m_\perp$  slopes. In the common  $p_\perp$  range of WA97 and NA49 experiments the transverse mass spectrum of  $\Lambda$  and  $\bar{\Lambda}$  obtained by NA49 is very well describe by an exponential [14]. A thermal model motivated fit of the inverse slope (temperature) yields  $T_\perp^\Lambda = 284 \pm 15$  MeV and  $T_\perp^{\bar{\Lambda}} = 282 \pm 20$  MeV. This is consistent with the mid-rapidity proton and antiproton slope of the NA44 experiment:  $T_p = 289 \pm 7$  MeV and  $T_{\bar{p}} = 278 \pm 9$  MeV. For  $\Xi + \bar{\Xi}$  a consistent value  $T_\Xi = 290$  MeV is also quoted by the NA49–collaboration [15]. We note that because the baryon masses are large, all these slopes are at relatively high  $m_\perp > 1.3$  GeV (for nucleons, in NA44,  $m_\perp > 1$  GeV). Systematically smaller inverse-transverse slopes are reported at smaller  $m_\perp$ , for kaons  $T_\perp^K \simeq 213$ – $224$  MeV for  $0.7 < m_\perp < 1.6$  GeV in NA49 [14] and  $T_\perp^{K^+} = 234 \pm 6$ ,  $T_\perp^{K^-} = 235 \pm 7$  MeV in NA44 [17]; and 155–185 MeV for  $\pi$ , [14, 17], depending on the range of  $p_\perp$ , but here we have to remember that pions are known to arise primarily from resonance decays. An increase of  $T$  with  $m_\perp$  is most naturally associated with the effects of transverse flow of the source.

## 3 Strangeness Production in QGP

### 3.1 Thermal reaction rates

We use two particle collision processes to evaluate thermal flavor production in QGP, as described in section 6 in Ref. [7], see also Ref. [21]. Recent results about strong interaction reaction rates constrain to sufficient precision the coupling strength  $\alpha_s(\mu)$ , however considerable uncertainty still remains, in particular in regard of strange quark mass scale  $m_s(\mu)$ , as well as systematic uncertainty related to applications of QCD to soft (less than 1 GeV) processes.

To determine these two QCD parameters ( $\alpha_s$  and  $m_s(\mu)$ ), we will use the renormalization group functions  $\beta$  and  $\gamma_m$ :

$$\mu \frac{\partial \alpha_s}{\partial \mu} = \beta(\alpha_s(\mu)), \quad \mu \frac{\partial m}{\partial \mu} = -m \gamma_m(\alpha_s(\mu)). \quad (9)$$

We use the perturbative power expansion in  $\alpha_s$ :

$$\begin{aligned} \beta^{\text{pert}} &= \alpha_s^2 \left[ b_0 + b_1 \alpha_s + b_2 \alpha_s^2 + \dots \right], \\ \gamma_m^{\text{pert}} &= \alpha_s \left[ c_0 + c_1 \alpha_s + c_2 \alpha_s^2 + \dots \right], \end{aligned} \quad (10)$$

For the SU(3)-gauge theory with  $n_f$  fermions the first two terms are renormalization scheme independent, and we include in our calculations the next three ‘loop’ term as well, which is renormalization scheme dependent, evaluated in the MS-scheme [22].

$$b_0 = \frac{1}{2\pi} \left( 11 - \frac{2}{3} n_f \right), \quad b_1 = \frac{1}{4\pi^2} \left( 51 - \frac{19}{3} n_f \right), \quad (11)$$

$$b_2 = \frac{1}{64\pi^3} \left( 2857 - \frac{5033}{9} n_f + \frac{325}{27} n_f^2 \right),$$

$$c_0 = \frac{2}{\pi}, \quad c_1 = \frac{1}{12\pi^2} \left( 101 - \frac{10}{3} n_f \right), \quad (12)$$

$$c_2 = \frac{1}{32\pi^3} \left( 1249 - \left( \frac{2216}{27} + \frac{160}{3} \zeta(3) \right) n_f - \frac{140}{81} n_f^2 \right).$$

The numerical influence of the third order term is nearly negligible for  $\mu > 1$  GeV, and it serves to stabilize our numerical solutions in the infrared domain. For this reason, we did not introduce the scheme dependent cross section to make the physical process rates exactly calculation scheme independent.

We use, in this report, the August 1996 World average [23]:  $\alpha_s(M_Z) = 0.118$  for which the estimated error is  $\pm 0.003$ . This value is sufficiently precise to eliminate most of the uncertainty that has befallen much of our earlier studies [7, 21]. First equation in (9) is numerically integrated beginning with an initial value of  $\alpha_s(M_Z) = 0.118$  and result is shown in the top portion of Fig. 3 (thick solid line). The thin solid line present results for  $\alpha_s(M_Z) = 0.115$  till recently the preferred result in some analysis, especially those at lower energy scale. The variation of  $\alpha_s$  with the energy scale is substantial, and in particular we note the rapid change at and below  $\mu = 1$  GeV, where the strange quark flavor formation occurs in hot QGP phase formed in present day experiments at 160–200A GeV (SPS). Clearly, use of constant value of  $\alpha_s$  is hardly justified, and the first order approximation often used

$$\alpha_s(\mu) \equiv \frac{2b_0^{-1}(n_f)}{\ln(\mu/\Lambda_0(\mu))^2}, \quad (13)$$

leads to a strongly scale dependent  $\Lambda_0(\mu)$  shown in the middle section of Fig. 3.

With  $\alpha_s(\mu)$  from the solutions described above, we integrate the running of the quark masses, the second equation in (9). Because the running mass equation is linear in  $m$ , it is possible to determine the universal quark mass scale factor

$$m_r = m(\mu)/m(\mu_0). \quad (14)$$

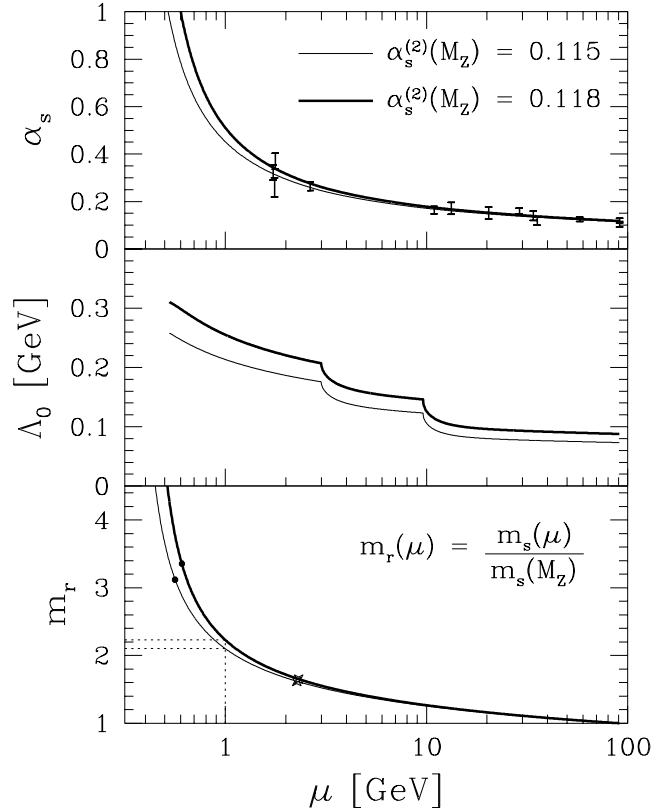


Figure 3:  $\alpha_s(\mu)$  (top section); the equivalent parameter  $\Lambda_0$  (see Eq. 13, middle section) and  $m_r(\mu) = m(\mu)/m(M_Z)$  (bottom section) as function of energy scale  $\mu$ . Initial value  $\alpha_s(M_Z) = 0.118$  (thick solid lines) and  $\alpha_s(M_Z) = 0.115$  (thin solid lines). In lower section the dots indicate the strangeness pair production thresholds for  $m_s(M_Z) = 90$  MeV, while crosses indicate charm pair production thresholds for  $m_c(M_Z) = 700$  MeV.

Since  $\alpha_s$  refers to the scale of  $\mu_0 = M_Z$ , it is a convenient reference point also for quark masses. As seen in the bottom portion of Fig. 3, the change in the quark mass factor is highly relevant, since it is driven by the rapidly changing  $\alpha_s$  near to  $\mu \simeq 1$  GeV. For each of the different functional dependences  $\alpha_s(\mu)$ , we obtain a different function  $m_r$ . Given these results, we find that for  $\alpha_s = 0.118$  and  $m_s(M_Z) = 90 \pm 18$  MeV a low energy strange quark mass  $m_s(1 \text{ GeV}) \simeq 200 \pm 40$  MeV, in the middle of the standard range  $100 < m_s(1 \text{ GeV}) < 300$  MeV. Similarly we consider  $m_c(M_Z) = 700 \pm 50$  MeV, for which value we find the low energy mass  $m_c(1 \text{ GeV}) \simeq 1550 \pm 110$  MeV, at the upper (conservative for particle production yield) end of the standard range  $1 < m_c(1 \text{ GeV}) < 1.6$  MeV.

There is another (nonperturbative) effect of running mass, related to the mass at threshold for pair production  $m_i^{\text{th}}$ ,  $i = s, c$ , arising from the solution of:

$$m_i^{\text{th}}/m_i(M_Z) = m_r(2m_i^{\text{th}}). \quad (15)$$

This effect stabilizes strangeness production cross section in the infrared: below  $\sqrt{s} = 1$  GeV the strange quark mass increases rapidly and the threshold mass is considerably greater than  $m_s(1 \text{ GeV})$ . We obtain the threshold values  $2m_s^{\text{th}} = 611$  MeV for  $\alpha_s(M_Z) = 0.118$  and  $2m_s^{\text{th}} = 566$  MeV for  $\alpha_s(M_Z) = 0.115$ . Both values are indicated by the black dots in Fig. 3. For charm, the

running mass effect plays differently: since the mass of charmed quarks is listed in tables for  $\mu = 1$  GeV, but the value of the mass is above 1 GeV, the production threshold mass is smaller than the listed value  $m_c(1 \text{ GeV})$ . For  $m_c(M_Z) = 700$  MeV the production threshold is found at  $\sim 2m_c^{\text{th}} \simeq 2.3$  GeV rather than 3.1 GeV that would have been naively expected. This reduction in threshold enhances thermal production of charm, especially so at low temperatures. The significance of the running of the charmed quark mass cannot be stressed enough, especially for thermal charm production occurring in foreseeable future experiments well below threshold, which amplifies the importance of exact value of  $m_c$ .

The thermal production rates are obtained from thermal average of the cross section:

$$\begin{aligned} A_s &\equiv A_{gg} + A_{u\bar{u}} + A_{d\bar{d}} + \dots \\ &= \int_{4m_s^2}^{\infty} ds 2s \delta(s - (p_1 + p_2)^2) \int \frac{d^3 p_1}{2(2\pi)^3 E_1} \int \frac{d^3 p_2}{2(2\pi)^3 E_2} \\ &\quad \times \left[ \frac{1}{2} g_g^2 f_g(p_1) f_g(p_2) \bar{\sigma}_{gg}(s) + n_f g_q^2 f_q(p_1) f_{\bar{q}}(p_2) \bar{\sigma}_{q\bar{q}}(s) + \dots \right]. \end{aligned} \quad (16)$$

The dots indicate that other mechanisms may contribute to strangeness production. The particle distributions  $f_i$  are in our case thermal Bose/Fermi functions (for fermions with  $\lambda_q = 1.5$ ), and  $g_q = 6$ ,  $g_g = 16$ . For strangeness production  $n_f = 2$ , and for charm production  $n_f = 3$ . The generic angle averaged two particle cross section for (heavy) flavor production processes  $g + g \rightarrow f + \bar{f}$  and  $q + \bar{q} \rightarrow f + \bar{f}$ , are

$$\bar{\sigma}_{gg \rightarrow f\bar{f}} = \frac{2\pi\alpha_s^2}{3s} \left[ \left( 1 + \frac{4m_f^2}{s} + \frac{m_f^4}{s^2} \right) \tanh^{-1} W(s) - \left( \frac{7}{8} + \frac{31m_f^2}{8s} \right) W(s) \right], \quad (17)$$

$$\bar{\sigma}_{q\bar{q} \rightarrow f\bar{f}} = \frac{8\pi\alpha_s^2}{27s} \left( 1 + \frac{2m_f^2}{s} \right) W(s), \quad (18)$$

where  $W(s) = \sqrt{1 - 4m_f^2/s}$ , and both the QCD coupling constant  $\alpha_s$  and flavor quark mass  $m_f$  are as determined above.

From the invariant rate we obtain the strangeness relaxation time  $\tau_s$  shown in Fig. 4, as function of temperature:

$$\tau_s \equiv \frac{1}{2} \frac{\rho_s^\infty(\tilde{m}_s)}{(A_{gg} + A_{qq} + \dots)}. \quad (19)$$

Note that here yet unaccounted for processes, such as the odd-order in  $\alpha_s$  would add to the production rate incoherently, since they can be distinguished by the presence of incoming/outgoing gluons. Thus the current calculation offers an upper limit on the actual relaxation time, which may still be smaller. In any case, the present result suffices to confirm that strangeness will be very near to chemical equilibrium in QGP formed in collisions of large nuclei.

We show in Fig. 4 the impact of a 20% uncertainty in  $m_s(M_Z)$ , indicated by the hatched areas. This uncertainty is today much larger compared to the uncertainty that arises from the recently improved precision of the strong coupling constant determination [23]. We note that the calculations made at fixed values  $\alpha_s = 0.5$  and  $m_s = 200$  MeV [24] (dotted line in Fig. 4) are well within the band of values related to the uncertainty in the strange quark mass.

Since charm is somewhat more massive compared to strangeness, there is still less uncertainty arising in the extrapolation of the coupling constant. Also the systematic uncertainty related to the soft gluons (odd- $\alpha_s$ ) terms are smaller, and thus the relaxation times  $\tau_c$ , we show

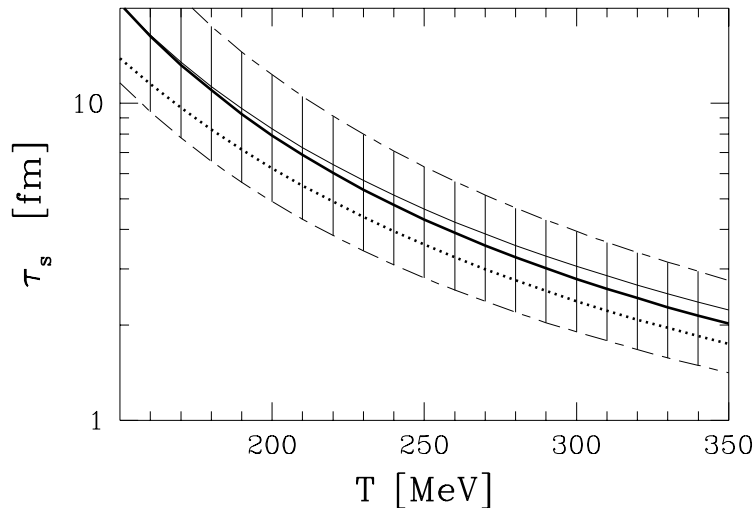


Figure 4: QGP strangeness relaxation time, for  $\alpha_s(M_Z) = 0.118$ , (thick line) and  $= 0.115$  (thin line);  $m_s(M_Z) = 90$  MeV. Hatched areas: effect of variation of strange quark mass by 20%. Dotted: comparison results for fixed  $\alpha_s = 0.5$  and  $m_s = 200$  MeV.

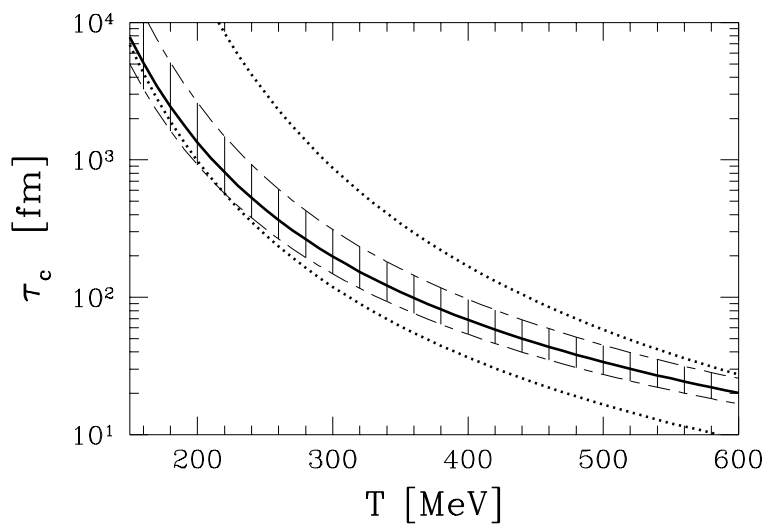


Figure 5: Solid lines: thermal charm relaxation constant in QGP, calculated for running  $\alpha_s(M_Z) = 0.115$ ;  $0.118$ , (indistinguishable),  $m_c(M_Z) = 700$  MeV. Lower dotted line: for fixed  $m_c = 1.1$  GeV,  $\alpha_s = 0.35$ ; upper dotted line: for fixed  $m_c = 1.5$  GeV,  $\alpha_s = 0.4$ . Hatched area: effect of variation  $m_c(M_Z) = 700 \pm 50$  MeV

in Fig. 5, are considerably better defined compared to  $\tau_s$ . There is also less relative uncertainty in the value of charm mass. We show in Fig. 5 (dotted lines) the fixed  $m_c, \alpha_s$  results with parameters selected to border high and low  $T$  limits of the results presented. It is difficult to find a good comparative behavior of  $\tau_c$  using just one set of  $m_c$  and  $\alpha_s$ . This may be attributed to the importance of the mass of the charmed quarks, considering that the threshold for charm production is well above the average thermal collision energy, which results in emphasis of the effect of running charm mass. In the high  $T$  limit, the choice (upper dotted line in Fig. 5)  $m_c = 1.5$  GeV,  $\alpha_s = 0.4$  is appropriate, while to follow the result at small  $T$  (lower dotted line in Fig. 4) we take a much smaller mass  $m_c = 1.1$  GeV,  $\alpha_s = 0.35$ .

We recall that the equilibrium distribution is result of Boltzmann equation description of two body collisions. Thus the mass arising in the equilibrium density  $\rho_s^\infty$  in Eq. (19), is to be taken at the energy scale of the average two parton collision. We adopt for this purpose a fixed value  $\tilde{m}_s = 200$  MeV, and observe that in the range of temperatures here considered the precise value of the mass is insignificant, since the quark density is primarily governed by the  $T^3$  term in this limit, with finite mass correction being  $\mathcal{O}(10\%)$ . The situation is less clear for charm relaxation, since the running of the mass should have a significant impact. Short of more complete kinetic treatment, we used  $m_c \simeq 1.5$  GeV in order to establish the reference density  $\rho_c^\infty$  in Eq. (19).

### 3.2 Strangeness evolution and hadronization

Given the improved relaxation times we proceed as in Ref. [7] to determine the two important strangeness observables ( $\gamma_s, N_s/B$ ) under conditions applicable for the SPS reactions. In order to compute the production and evolution of strangeness (and charm) flavor a more specific picture of the temporal evolution of dense matter is needed. In a simple, qualitative description, we assume that the hot, dense matter is homogeneous. We consider that, in Pb–Pb collisions at SPS, the radial expansion is the dominant factor for the evolution of the fireball properties such as temperature/energy density and lifetime of the QGP phase. The expansion dynamics follows from two assumptions:

- the (radial) expansion is entropy conserving, thus the volume and temperature satisfy

$$V \cdot T^3 = \text{Const.} \quad (20)$$

- the surface flow velocity is given by the sound velocity in a relativistic gas

$$v_f = 1/\sqrt{3}. \quad (21)$$

These two assumption imply the following explicit forms for the radius of the fireball and its average temperature:

$$R = R_{\text{in}} + \frac{1}{\sqrt{3}}(t - t_{\text{in}}), \quad T = \frac{T_{\text{in}}}{1 + (t - t_{\text{in}})/\sqrt{3}R_{\text{in}}}. \quad (22)$$

We shall see below that if QGP formation is involved, a fit of strange antibaryons data either leads to direct emission before expansion, or to emission from a surface expanding with just this velocity  $v_f$ .

The initial conditions have been determined such that the energy per baryon is given by energy and baryon flow, and the total baryon number is  $\eta(A_1 + A_2)$ , as stopped in the interaction

Table 1: The initial conditions for S–Pb/W at 200A GeV and Pb–Pb at 158A GeV for different stopping values  $\eta$ .

	$t_{\text{in}}$ [fm]	$\eta$	$R_{\text{in}}$ [fm]	$T_{\text{in}}$ [MeV]	$\lambda_q$
S–Pb/W	1	0.35	3.3	280	1.5
	1	0.5	3.7	280	1.5
Pb–Pb	1	0.5	4.5	320	1.6
	1	0.75	5.2	320	1.6

 Table 2:  $\gamma_s$  and  $N_s/B$  in S–W at 200A GeV and Pb–Pb at 158A GeV for different stopping values of baryonic number and energy  $\eta_B = \eta_E$ ; computed for strange quark mass  $m_s(1\text{GeV}) = 200 \pm 40$  MeV,  $\alpha_s(M_Z) = 0.118$ .

$E_{\text{lab}}$	S–W at 200A GeV		Pb–Pb at 158A GeV	
$\eta_B = \eta_E$	0.35	0.5	0.5	0.75
$\gamma_s$	$0.53 \pm 0.14$	$0.65 \pm 0.15$	$0.69 \pm 0.15$	$0.76 \pm 0.16$
$N_s/B$	$0.67 \pm 0.16$	$0.70 \pm 0.16$	$0.954 \pm 0.20$	$0.950 \pm 0.20$

region. They are shown in table 1. The radius are for zero impact parameter. For this, equations of state of the QGP are needed, and we have employed our model [25] in which the perturbative correction to the number of degrees of freedom were incorporated along with thermal particle masses.

Allowing for dilution of the phase space density in expansion, we integrate a population equations describing the change in  $\gamma_s(t)$  [7]:

$$\frac{d\gamma_s}{dt} = \left( \gamma_s \frac{\dot{T} m_s}{T^2} \frac{d}{dx} \ln x^2 K_2(x) + \frac{1}{2\tau_s} [1 - \gamma_s^2] \right). \quad (23)$$

Here  $K_2$  is a Bessel function and  $x = m_s/T$ . Note that even when  $1 - \gamma_s^2 < 1$  we still can have a positive derivative of  $\gamma_s$ , since the first term on the right hand side of Eq. (23) is always positive, both  $\dot{T}$  and  $d/dx(x^2 K_2)$  being always negative. This shows that dilution due to expansion effects in principle can make the value of  $\gamma_s$  rise above unity.

Given the relaxation constant  $\tau_s(T(t))$ , these equations can be integrated numerically, and we can obtain for the two currently explored experimental systems the values of the two observables,  $\gamma_s$  and  $N_s/B$ , which are given in table 2. There is a considerable uncertainty due to the unknown mass of strange quarks. However, since this is a not statistical but systematic uncertainty depending nearly alone on the value of the strange quark mass parameter, all the results presented will shift together. We note further that there seems to be very little dependence on the stopping fractions in the yield of strange quarks per baryon  $N_s/B$ . Thus if the expected increase in stopping is confirmed, we should also expect a small increase by 15% in specific strangeness yield.

## 4 QGP Thermo-chemical Freeze-out Parameters From Pb–Pb

## 4.1 Primordial emission scenario

We next introduce all the model parameters used in the fit of the particle ratios, not all will be required in different discussions of the experimental data. For more details about the thermochemical parameters we refer to the extensive discussion in the earlier study of S–S and S–W data [7]. The key parameters are:

1)  $T_f$  is the formation/emission/freeze-out temperature, depending on the reaction model.  $T_f$  enters in the fit of abundance ratios of unlike particles presented within a fixed  $p_\perp$  interval. The temperature  $T_f$  can in first approximation be related to the observed high- $m_\perp$  slope  $T_\perp$  by:

$$T_\perp \simeq T_f \frac{1 + v_\perp}{\sqrt{1 - v_\perp^2 - v_\parallel^2}}. \quad (24)$$

In the central rapidity region the longitudinal flow  $v_\parallel \simeq 0$ , in order to assure symmetry between projectile and target. Thus as long as  $T_f < T_\perp$ , we shall use Eq. (24) setting  $v_\parallel = 0$  to estimate the transverse flow velocity  $v_\perp$  of the source.

2)  $\lambda_q$  is the light quark fugacity. We initially used in our fits both  $u$ ,  $d$ -flavor fugacities  $\lambda_u$  and  $\lambda_d$ , but we saw that the results were equally adequate without allowing for up-down quark asymmetry, using the geometric average  $\lambda_q = \sqrt{\lambda_u \lambda_d}$ ; moreover the fitted up-down quark fugacity asymmetry was found as expected in our earlier analytical studies [26].

3)  $\lambda_s$  is the strange quark fugacity. A source in which the carriers of  $s$  and  $\bar{s}$  quarks are symmetric this parameter should have the value  $\lambda_s \simeq 1$ , in general in a re-equilibrated hadronic matter the value of  $\lambda_s$  can be determined requiring strangeness conservation.

4)  $\gamma_s$  is the strange phase space occupancy. Due to rapid evolution of dense hadronic matter it is in general highly unlikely that the total abundance of strangeness can follow the rapid change in the conditions of the source, and thus in general the phase space will not be showing an overall abundance equilibrium corresponding to the momentary conditions.

5) We also show when appropriate in table 3 the parameter  $R_C^s$  describing the relative off-equilibrium abundance of strange mesons and baryons, using thermal equilibrium abundance as reference. This parameter is needed, when we have constraint on the strangeness abundance and/or when we address the abundance of mesons since there is no a priori assurance that the relative production/emission strength of strange mesons and baryons should proceed according to relative strength expected from thermal equilibrium. Moreover, it is obvious that even if reequilibration of particles in hadronic gas should occur, this parameter will not easily find its chemical equilibrium value  $R_C^s = 1$  as we alluded to in section 1. However, due to reactions connecting strange with non-strange particles we expect  $R_C^s = R_C$ , where  $R_C$  is the same ratio for non-strange mesons and baryons, using thermal abundance as reference. The value of  $R_C > 1$  implies meson excess abundance per baryon, and thus excess specific entropy production, also expected in presence of color deconfinement [8].

The relative number of particles of same type emitted at a given instance by a hot source is obtained by noting that the probability to find all the  $j$ -components contained within the  $i$ -th emitted particle is

$$N_i \propto \gamma_s^k \prod_{j \in i} \lambda_j e^{-E_j/T}, \quad (25)$$

and we note that the total energy and fugacity of the particle is:

$$E_i = \sum_{j \in i} E_j, \quad \lambda_i = \prod_{j \in i} \lambda_j. \quad (26)$$

Table 3: Values of fitted statistical parameters within thermal model, for 158A GeV Pb–Pb strange particle production data. Superscript star ‘\*’: a fixed input value for equilibrium hadronic gas; subscript ‘|c’: value is result of the imposed strangeness conservation constraint.  $\chi^2$  is the total relative square error of the fit for all data points used. First result line: direct emission QGP model, no meson to baryon ratio fit. Second line: same, but with strangeness conservation yielding  $\lambda_s$ , and  $R_C^s$  variable. Line three: as in line two, in addition the meson to baryon ratio Eq. (8) is fitted. Line four: hadronic gas fit including the ratio Eq. (8).

$T_f[MeV]$	$\lambda_q$	$\lambda_s$	$\gamma_s$	$R_C^s$	$\chi^2$
$272 \pm 74$	$1.50 \pm 0.07$	$1.14 \pm 0.04$	$0.63 \pm 0.10$	—	1.0
$272 \pm 74$	$1.50 \pm 0.08$	$1.14 _c$	$0.63 \pm 0.10$	$4.21 \pm 1.88$	1.0
$151 \pm 10$	$1.54 \pm 0.08$	$1.13 _c$	$0.91 \pm 0.09$	$0.85 \pm 0.22$	1.5
$155 \pm 7$	$1.56 \pm 0.09$	$1.14 _c$	1*	1*	7.6

The strangeness occupancy  $\gamma_s$  enters Eq. (25) with power  $k$ , which equals the number of strange and antistrange quarks in the hadron  $i$ . With  $E_i = \sqrt{m_i^2 + p^2} = \sqrt{m_i^2 + p_\perp^2} \cosh y$  we integrate over the transverse momentum range as given by the experiment (here  $p_\perp > 0.6$  GeV) taking central rapidity region  $y \simeq 0$  to obtain the relative strengths of particles produced. We then allow all hadronic resonances to disintegrate in order to obtain the final relative multiplicity of ‘stable’ particles required to form the observed particle ratios. This approach allows to compute the relative strengths of strange (anti)baryons both in case of surface emission and equilibrium disintegration of a particle gas since the phase space occupancies are in both cases properly accounted for by Eq. (25). The transverse flow phenomena enter in a similar fashion into particles of comparable mass and are not expected to influence particle ratios. Finally we note that particles which are easily influenced by the medium, such as  $\phi$ , require a greater effort than this simple model, and are also not explored in depth here.

We obtain the least square fit for the eight above reported (anti)baryon ratios. Our first approach is motivated by the reaction picture consisting of direct emission from the QGP deconfined fireball. The value of statistical parameters controlling the abundances are thus free of constraints arising in an equilibrated hadronic gas (HG) state [26]. The fitted thermal parameters are presented in the first line of table 3 along with the total  $\chi^2$  for the eight ratios. The fit is quite good, the error shown corresponds to the total accumulated error from 8 measurements; even if one argues that it involves 4 parameters to describe 5 truly independent quantities, the statistical significance is considerable, considering that 8 different measurements are included. Such a free fit does not know that we are expecting that the final state comprises a balance  $\langle s - \bar{s} \rangle = 0$ . In order to estimate what would be implied by strangeness conservation constraint among emitted hadrons we present in second line of table 3 the result of a fit assuming that the value of  $\lambda_s$  is result of the conservation constraint  $\langle s - \bar{s} \rangle = 0$ , and allowing  $R_C^s \neq 1$ , for there should be no chemical equilibrium among the emitted strange mesons and strange baryons in a sudden and early QGP disintegration. The statistical error is found the same as in line 1, since this approach substitutes one parameter ( $\lambda_s$ ) by another ( $R_C^s$ ). The implication of this fit is that there must be either an excess of strange mesons or depletion of strange baryons compared to thermal equilibrium expectation, since as we recall  $R_C^s = C_M^s/C_B^s$  with  $C_i$  being the yield of particles, normalized to one for thermal equilibrium yield. In any case we see that strange meson excess is required, which is consistent with excess of entropy production.

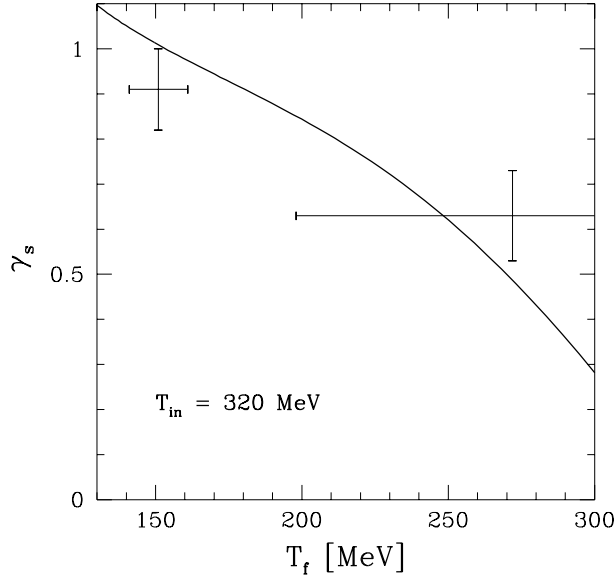


Figure 6: QGP strangeness occupancy  $\gamma_s$  as function of temperature  $T_f$  at time of particle production, for initial temperature  $T_{\text{in}} = 320$  MeV, with  $\gamma_s(T_{\text{in}}) = 0.1$ .

The errors seen in the two first lines of table 3 on the statistical parameters arise in part from strong correlations among them. In particular the very large error in  $T_f$  arise from the 80% anti-correlation with  $\gamma_s$ . However, some further information about the relation of  $T_f$  and  $\gamma_s$  may be garnered from theoretical considerations. We evaluate using our dynamical strangeness production model in QGP how the value of  $\gamma_s$  depends on the temperature of particle production  $T_f$ . The most important parameter in such a theoretical evaluation is the initial temperature at which the deconfined phase is created. As noted above, we estimated this temperature at  $T_{\text{in}} = 320$  MeV [25]. Further uncertainty of the calculation arises from the strange quark mass taken here to be  $m_s(1 \text{ GeV}) = 200$  MeV. We recall that the strength of the production rate is now sufficiently constrained by the measurement of  $\alpha_s(M_Z)$ . We choose a geometric size which comprises a baryon number  $B = 300$  at  $\lambda_q \simeq 1.5$ , and have verified that our result will be little dependent on small variations in  $B$ . We show in Fig. 6 how the computed  $\gamma_s$  depends on formation temperature  $T_f$ . The cross to the right shows our fitted value from line 1 or 2 in table 3. It is gratifying to see that it is consistent with the theoretical expectation for early formation of the strange (anti)baryons. The relative smallness of  $\gamma_s$ , despite the high strangeness yield, is clearly related to the high temperature of particle production.

The relatively high value of temperature  $T_f$  we obtained in the QGP reaction picture with primordial particle emission is in qualitative agreement with the experimental inverse slope data we discussed in section 2. We are thus led to the conclusion that as far as the fitted temperatures and slopes are concerned, it is possible that the high  $m_{\perp}$  strange (anti)baryons we have described could have been emitted directly from a primordial (deconfined) phase before it evolves into final state hadrons.

Is QGP primordial emission hypothesis also consistent with the chemical fugacities we have obtained? The chemical condition is fixed to about 5% precision, and there is 40% anti-correlation between the two fugacities  $\lambda_q$  and  $\lambda_s$ . The information that  $\lambda_s \neq 1$  is contained in at least two particle abundances; arbitrary manipulation of the reported yields of one particle

abundance did not reduce the value  $\lambda_s$  to unity. Since  $\lambda_s \neq 1$  by 4 s.d. it is highly unlikely that  $\lambda_s = 1$  is found after more data is studied. While one naively expects  $\lambda_s^{\text{QGP}} = 1$ , to assure the strangeness balance  $\langle s - \bar{s} \rangle = 0$ , there must be a small deviations from this value, even if the emitted particles were to reach asymptotic distances without any further interactions: in presence of baryon density the deconfined state is not fully symmetric under interchange of particles with antiparticles. A possible mechanism to distinguish the strange and anti-strange quarks arises akin to the effect considered for the  $K^-/K^+$  asymmetry in baryonic matter [27, 28]: there is asymmetric scattering strength on baryon density  $\nu_b$  which causes presence of a mean effective vector potential  $W$ . Similarly, strange quark interaction with baryon density would lead to a dispersion relation

$$E_{s/\bar{s}} = \sqrt{m_s^2 + p^2} \pm W, \quad (27)$$

and this requires in the statistical approach that the Fermi distribution for strange and anti-strange quarks acquires a compensating fugacity  $\lambda_{s,\bar{s}} = e^{\pm W/T}$  to assure strangeness balance in the deconfined phase. In linear response approach  $W \propto \nu_b$  consistent with both  $W$  and baryon density  $\nu_b = (n_q - n_{\bar{q}})/3$ , being fourth component of a Lorenz-vector. It is clear for intuitive reasons, as well as given experimental observations, that the baryon stopping and thus density increases considerably comparing the S and Pb induced reactions in the energy domain here considered. We also recall that in S–W reactions  $\lambda_s^S \simeq 1.03 \pm 0.05$  [29]. Should in the dense matter fireball the baryon density  $\nu_b$  grow by factor 2–4 as the projectile changes from S to Pb, this alone would consistently explain the appearance of the value  $\lambda_s = 1.14 \pm 0.04$  obtain using  $W \propto \nu_b$  scaling. It is worth noting that the value  $W \simeq 38$  MeV suffices here. Note also that the Coulomb potential effect on the charge of the strange quarks is of opposite magnitude and about 1/5–1/6 of the here required strength.

## 4.2 Late emission scenario: HG with or without QGP?

A generally favored picture of particle production involves flow expansion of the primordial phase till a transition temperature is reached, at which time the final state hadrons are produced, and soon thereafter freeze out. These particles may directly reach a detector or reequilibrate and appear to the observer as if emitted from a HG phase, except that entropy/strangeness excess effect should remain. In order to force our data fit to converge to such a late particle production scenario we introduce the experimental result, which was essential for such an argument in the S–Pb induced reactions. The quantity of interest is ratio of particle yields between particles of very different mass. Thus in lines 3, 4 in table 3 we include in the fit also our estimate of the hyperon to kaon ratio Eq. (8), thus altogether we now fit 9 data points.

Our approach in the third line corresponds to a freeze-out from ‘cold’ QGP phase, in that we allow the abundance parameters  $\gamma_s$  and  $R_C^s$  to deviate from HG equilibrium values. We note that this cold-QGP alternative has a very comparable statistical significance as the hot-QGP. Given the low temperature and high  $m_\perp$  inverse slopes we must have considerable transverse flow. The computed flow velocity at freeze-out is  $v_f = 0.51c$ . This is just below the relativistic sound velocity  $v_s = 1/\sqrt{3} = 0.58$ , which we have assumed. In Fig. 6 the cross to the left shows the result of the fit we just described; allowing for potentially smaller expansion velocity and all the above discussed uncertainties in the computation, this result must also be seen as a very good agreement between the result of data fit and the theoretical calculation. This also means

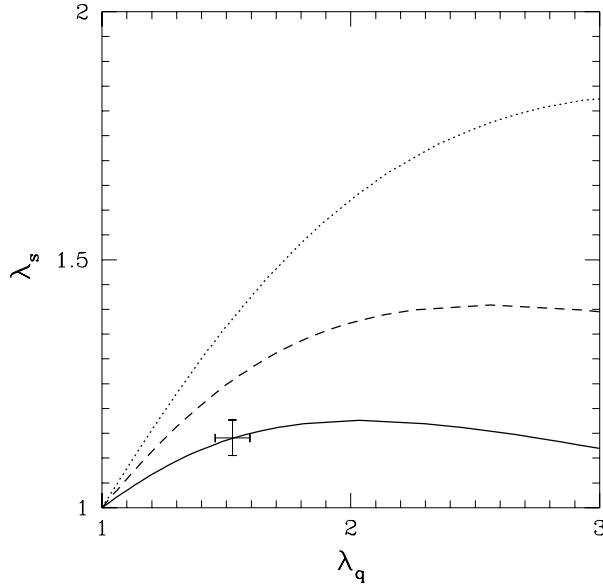


Figure 7: Strangeness conservation constraint in HG as function of freeze-out  $\lambda_q$ : the lines correspond to different freeze-out temperatures  $T_f$  (solid 160 MeV, dashed 140 MeV and dotted 120 MeV). The cross corresponds to the chemical freeze-out we determined above.

that we cannot distinguish in the present data between early formation of strange antibaryons and an expansion model followed by direct global hadronization.

Since the fitted values of  $\gamma_s$  and  $R_C^s$  allow the HG equilibrium, we attempt such a fit in line 4, where the particle yields are fitted constrained for HG equilibrium, and we use strangeness conservation to evaluate the strangeness fugacity  $\lambda_s$ . We show the result of the fit in the last line of table 3 and in particular we note:

$$\begin{aligned}
 T_f &= 155 \pm 7 \text{ MeV}, & \rightarrow v_\perp \simeq 0.5 \simeq v_s; \\
 \lambda_q &= 1.56 \pm 0.09, & \rightarrow \lambda_s = 1.14; \\
 \chi^2/9 &= 0.84, & \rightarrow \text{C.L.} > 60\%.
 \end{aligned}
 \tag{28}$$

We recall that the baryochemical potential is given in terms of  $T$  and  $\lambda_q$ , specifically  $\mu_b = 3T \ln \lambda_q$ , and we find  $\mu_b = 204 \pm 10$  MeV in this hadronic gas condition. We note that while the quality of the fit has degraded, it still has considerable statistical significance. It would appear to be a ‘good’ fit to the naked, unequipped eye.

Unlike S-induced reactions, the hypothesis of an equilibrated HG in the final state cannot be easily discarded in Pb–Pb collisions since the thermo-chemical parameters are extraordinarily consistent with this hypothesis and the principle of strangeness conservation, as we illustrate in Fig. 7. Here, the cross corresponds to the fitted properties of the particle source, while the lines correspond to the constraint of the HG gas source to yield  $\langle s - \bar{s} \rangle = 0$  at finite baryon density represented by the value of  $\lambda_q$ . Thus the strange quark fugacity is in general not zero and the cross falls just on freeze-out at  $T = 160$  MeV when the meson-baryon abundance is equilibrated. The slight difference in freeze-out value to results shown in last line of table 3 is result of using the WA97  $\bar{\Lambda}/\Lambda$  value Eq. (1) rather than the averred value Eq. (4).

If HG is indeed present in the final state, the proper interpretation of these data, and the likely reaction scenario, compatible with our earlier work on S induced reactions [7] is as fol-

lows; the relatively large fireball of dense and deconfined matter disintegrates and produces dense, confined hadronic gas in which strange particles have time to rescatter and to establish relative chemical equilibrium. A possible test of this hypothesis would be to see variation of the chemical parameters as the size of the fireball changes with impact parameter (centrality of collision) since reequilibration should diminish for small reaction volume. However, such data are presently not available, and there is no indication that indeed a change of the strange (anti)baryon yields occurs as the centrality of the interaction is reduced. On the other hand, the specific entropy and strangeness should comprise a signal of some new physics should formation and expansion of QGP phase, followed by reequilibration into HG phase, and freeze-out have occurred. We will now consider the magnitude of these effects:

### Strangeness reequilibration

When HG emerges from initial dense QGP phase, the number of strange quark pairs does not change, but the phase space density of strangeness changes, since the phases are different. Because the HG phase has generally a smaller phase space density of strangeness than QGP, to conserve strangeness, there will be a jump in the phase space occupancy  $\gamma_s$  during the transformation of QGP into HG, as there is a jump in the strange quark fugacity. The important point is that this could lead to significantly overpopulated HG phase ( $\gamma_s > 1$ ). This phenomenon can be easily quantified as follows: the observed value of  $\gamma_s^{\text{HG}}$  is related to the pre-phase change value  $\gamma_s^{\text{QGP}}$  by introducing the enhancement factor we wish to determine:

$$\gamma_s^{\text{HG}} \equiv F_\gamma \gamma_s^{\text{QGP}} \quad (29)$$

A simple way to compute the value of the saturation enhancement factor  $F_\gamma$  is to study the abundance of strangeness per baryon number before and after phase transition.

$$F_\gamma = \frac{s/b|_{\text{QGP}}}{s/b|_{\text{HG}}} = \frac{\gamma_s^{\text{QGP}}}{\gamma_s^{\text{HG}}} f(T_f, \lambda_q, \gamma_s^{\text{HG}}). \quad (30)$$

The last expression arises as follows: on the QGP side the abundance of strangeness is to a good approximation proportional to  $\gamma_s^{\text{QGP}}$  and is the integral of the strange quark phase space, we evaluate it assuming that  $m_s/T_{\text{QGP}} \simeq 1$ . There is no dependence on chemical properties of the plasma. On HG side, at freeze-out we have to evaluate the strangeness abundance from the strange particle partition function given in Eq. (16) of [26], supplemented by the now relevant term comprising  $s\bar{s}$ - $\eta$ ,  $\eta'$ ,  $\phi$  states and their resonances. The sum includes a terms proportional to  $(\gamma_s^{\text{HG}})^n$ , with  $n=1, 2, 3$ , indicating strangeness content of hadrons. The leading kaon and hyperon term is proportional to  $\gamma_s^{\text{HG}}$  and hence we have above result, Eq. (30). We thus obtain, combining Eqs. (29) and Eq. (30),

$$F_\gamma^2 = F_\gamma \frac{\gamma_s^{\text{HG}}}{\gamma_s^{\text{QGP}}} = \frac{s}{\gamma_s b} \Big|_{\text{QGP}} \cdot \frac{\gamma_s b}{s} \Big|_{\text{HG}}, \quad (31)$$

where the right hand side now compares the properties of the two phases at the boundary between them and we can evaluate it using the theoretical equations of state. In analyzes of an experiment we would take the freeze-out parameters determined by the fit to data.

We show, in Fig. 8, the strangeness enhancement factor as function of  $\lambda_q$  for several freeze-out temperatures  $T_f = 160, 140, 120$  MeV, with  $\lambda_s$  fixed by strangeness conservation constraint. We see that  $F_\gamma$  varies typically between 1.5 and 2, and is specifically 1.6 for the parameter rage

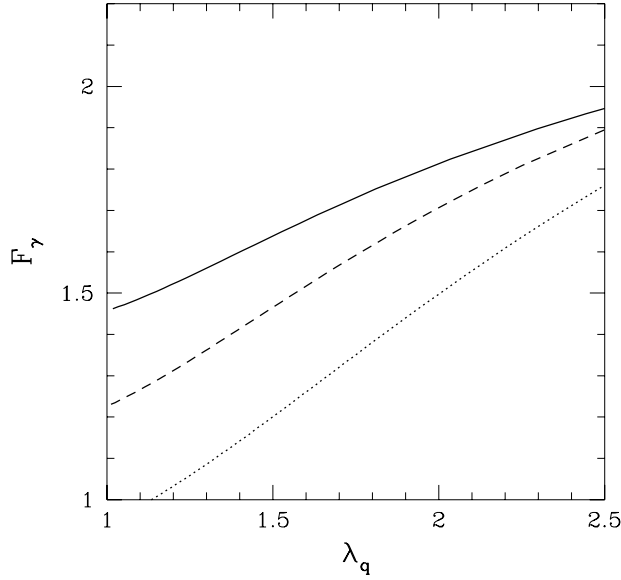


Figure 8: Strangeness phase space enhancement factor as function of HG freeze out  $\lambda_q$  for  $T_f = 160$  (solid line),  $T_f = 140$  (dashed line),  $T_f = 120$  (dotted line). Computed for  $\gamma_s^{\text{HG}} = 1$ ,  $m_s/T_{\text{QGP}} = 1$ , including in HG phase kaons, hyperons, cascades,  $\eta$ ,  $\phi$ ,  $\Omega$ , and imposing strangeness conservation constraint to determine  $\lambda_s$ .

of Pb–Pb collisions here discussed. This means that observing the value  $\gamma_s \simeq 1$  really means an underlying value  $\gamma_s^{\text{QGP}} \simeq 0.6$ . Conversely, should we be able to create a longer lived or hotter QGP state we could expect to observe in the HG phase  $\gamma_s^{\text{HG}}$  as large as 1.5–2. Such over-saturation of the phase space would be a rather strong smoking gun pointing to the formation of the QGP phase.

### Entropy and particle excess

Another way to argue for the formation of QGP in early stages of an expansion scenario of the fireball is to measure the specific entropy experimentally, for example by measuring the quantity

$$D_Q \equiv \left( \frac{dN^+}{dy} - \frac{dN^-}{dy} \right) / \left( \frac{dN^+}{dy} + \frac{dN^-}{dy} \right), \quad (32)$$

which we have shown to be a good measure of the entropy content [29]. We note that in the numerator of  $D_Q$  the charge of particle pairs produced cancels and hence this value is effectively a measure of the baryon number, but there is a significant correction arising from the presence of strange particles. The denominator is a measure of the total multiplicity — its value is different before or after disintegration of the produced unstable hadronic resonances. Using as input the distribution of final state particles as generated within the hadron gas final state it is found [8] that  $D_Q \cdot S/B$  is nearly independent of the thermal parameters and varies between 4.8, before disintegration of the resonances, to 3 after disintegration.

To obtain a measure of the particle excess, we show in Fig. 9 the specific entropy per baryon  $S/B$  content in dense hadronic matter as a function of light quark fugacity  $\lambda_q$ . The thick line addresses the deconfined QGP phase, the thin line the confined HG phase at  $T = 155$  MeV, with the strange quark fugacity  $\lambda_s$  being determined from the strangeness conservation

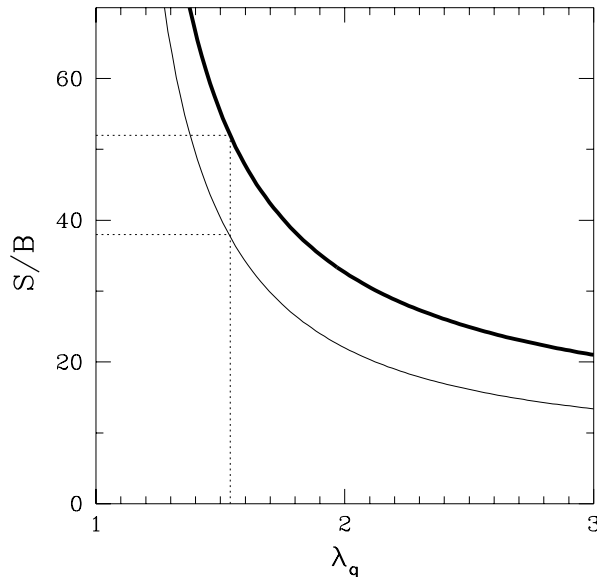


Figure 9: QGP (thick line) and HG (thin line,  $T = 155$  MeV) entropy per baryon  $S/B$  as function of light quark fugacity  $\lambda_q$ . Dotted lines guide the eye for the here interesting values.

condition. While the QGP result is largely independent of temperature (only other, aside of  $T$  dimensioned quantity, is  $m_s$ ), the HG result involves the values of all hadron masses and hence is dependent on  $T$ . The 12 units of entropy difference between the two phases for the here interesting range of fugacity  $\lambda_q = 1.5$ – $1.6$  implies that we should expect an excess of about 3 mesons per baryon if the deconfined phase is formed. We compare with a HG at  $T = 155$  MeV; should the HG phase of interest be hotter, this difference between QGP and HG grows, since the baryon density in HG grows much faster than entropy for the baryon mass is well below the temperature range and thus a change in the factor  $m_N/T$  matters, while the change in  $m_\pi/T$  is immaterial. In other work HG phase at 190 MeV is often considered, and there the difference between QGP and HG properties turns out to be as large as factor two [8].

## 5 QGP: Year 1997 or 2001?

In our view, strangeness and entropy results analyzed, here and earlier [7], are most consistent with the hypothesis that the same type of matter is formed in both S- and Pb-induced reactions, but that quite different ‘initial’ conditions are reached, specifically different energy density and very different baryon density. Moreover, the longitudinal flow, clearly visible in the S–S 200A GeV, in *e.g.*,  $\Lambda$ -rapidity spectra, is not seen in Pb–Pb reactions (see Fig. 1), but there could be strong transverse/radial flow driven by high internal pressure in the fireball, required to connect the low freeze-out temperature (see third and fourth fit of table 3) to the high inverse  $m_\perp$  slope, see Eq. (24). We also expect that the much greater volume occupied by the initially deconfined phase should enhance the reequilibration process of hadrons after freeze-out, furthering the approach to chemical equilibrium particle yields.

Given these considerable differences in reaction dynamics, it is surprising that the strange antibaryon yields from Pb–Pb reactions appear to be, at least on first sight, similar to the S–W/Pb or even S–S results. Our understanding and explanation of this phenomenon is that

the abundance (but not necessarily the spectrum) of relatively high  $m_{\perp}$  strange (anti)baryons is originating in a similar stage of a hot matter fireball. To this point we note that several *ad-hoc* mechanisms (such as, *e.g.*, ‘ropes’, ‘string fusion’, *etc.*) were proposed in literature aiming to explain the strange antibaryon yields in S–S/Ag/W/Pb reactions, and which should in case of Pb–Pb reactions yield even a greater strange antibaryon production anomaly, not seen in the experimental results known to us and described here.

At this point we wish to address another important experimental result which indeed shows considerable differences between S–A and Pb–Pb data [30]: the rate of absorption of the  $J/\Psi$ , per unit of size of the interaction region, is systematically enhanced when the reaction region is sufficiently large, as measured by transverse energy. We wish to interpret that exciting result in a slightly different manner than has been proposed before [31], in order to reconcile it with our claim that S– and Pb– induced reaction lead to the same type of (deconfined) dense primordial hadronic matter.

Seen in the CM-frame of reference for the Pb–Pb system, the produced  $J/\Psi$  is almost ‘at rest’ compared to the rapidly evolving, ‘light’ hadronic matter. In an idealized picture,  $J/\Psi$  sits still as it is banged on initially by quarks and gluons, and if reequilibration is occurring, also by individual hadrons. One of the results of this reaction picture is that we expect the  $m_{\perp}$  spectrum of  $J/\Psi$  to become thermal, since the particles hitting it are thermal; the other is that the observed absorption of  $J/\Psi$  is not a function of the size of the fireball, as  $J/\Psi$  does not take a straight path out of the production point through the surrounding matter. If it is moving out, it would be certainly not straight given the interactions with the medium; despite its great mass compared to massless quarks and gluons, the nonrelativistic thermal momentum of  $J/\Psi$ :  $p = \sqrt{3mT}$  is, at  $T = 250$  MeV, just twice as large as the thermal relativistic momentum of the light quarks and gluons,  $p \simeq 3T$ , which assures rapid thermalization of  $J/\Psi$ . In this approach  $J/\Psi$  absorption depends on how long it is exposed to interactions with hadronic matter in its various forms, perhaps most importantly with the color screening QGP phase, and the ‘anomalous’ suppression of  $J/\Psi$  in central Pb–Pb reactions simply implies that the large, dense hadronic fireball has an extended lifespan compared to peripheral Pb–Pb reactions or S– and p–induced reactions. Critical phenomena such as development of a ‘frozen’ HG envelope (expanding considerably slower) around the deconfined region could lead to the reported sudden change in  $J/\Psi$  suppression with  $E_{\perp}$ .

We would expect an equally sudden change as function of  $E_{\perp}$  of the chemical parameter  $\lambda_s$  since formation of a ‘frozen’ HG surface should also lead to strange (anti)baryon reequilibration in this matter envelope. A way to verify this hypothesis would be to show that, as function of Pb–Pb collision centrality, the strange quark fugacity drops (quite suddenly) from the HG equilibrium value to the QGP direct emission value  $\lambda_s \rightarrow 1$ , just at the same critical  $E_{\perp}$  noted in study of  $J/\Psi$  suppression.

We conclude that the appropriate source of strange particles in Pb–Pb collisions is an expanding QGP fireball, that undergoes a reequilibrating phase transformation, capable to delay its dissociation. This scenario represented in table 3, line 3, is as argued above qualitatively consistent with the anomalous  $J/\Psi$  suppression, provided that we do not model  $J/\Psi$  as escaping the reaction region, but instead see matter flowing out of the central formation region of the  $J/\Psi$ .

Let us stress again that in our here presented work, we did assume that thermal quark-gluon degrees of freedom are at origin of many of the hadronic particle production phenomena in relativistic hadron reactions. Many simple, but subtle experimental observations point in this

natural direction. For example, all so far studied  $m_{\perp}$  spectra in S- and Pb-induced reactions have the same shape for strange baryons and antibaryons of the same kind, and even for different kinds, where comparison can be made in same range of  $m_{\perp}$ . This is not an accident, but result of either complete thermal equilibrium, or of their origin in a thermal source composed of their constituents (quarks). Only a thermal quark liquid can deliver this result naturally.

Similarly, we take the presence of near chemical equilibrium of strangeness to be a signal of primordial QGP phase. The phase space occupancy factor expected in the QGP phase is of magnitude 0.6 and is enhanced by the lower strangeness density in the HG phase by a factor 1.5 to reach unity. The chemical parameters that are observed lead to abundance anomalies such as  $\bar{\Lambda}/\bar{p} > 1$ . There is a priori no reason for a HG state to reach condition amenable to this result, should it not arrive from a QGP state.

All told, we believe that the most simple and consistent reaction picture involves formation of deconfined phase of hadronic matter both in S- and Pb-induced reactions. The difference between both cases is that the former leads to a small enough fireball that can rapidly disintegrate under influence of the longitudinal flow and without forming an intermediate fully equilibrated HG phase. The Pb–Pb reactions, comprising five times the amount of matter, considerably higher energy density and much less longitudinal flow, appear to undergo a more protracted evolution history, and in particular they appear to pass through a stage of reequilibrated HG, before the strange antibaryons decouple (freeze-out) and stream freely to the detectors.

We have no idea how to describe the relativistic heavy ion hadron spectra data without invoking thermal quark-gluon fluid, commonly referred to as QGP. However, we have many more experiments and theoretical analysis to perform to be sure that we understand the reaction history and the properties of the bizarre liquid of quarks and gluons. The answer thus is, QGP is arriving in 1997, but needs to be properly dressed for more general presentation to the public.

## Acknowledgments:

One of us (J.R.) would like to thank the organizers of the XXXVII Zakopane Summer School, and in particular Jan Czyżewski and Jacek Wosiek, and Marja Czyż, for their great Polish hospitality during a most fruitful and interesting meeting.

## References

- [1] W. Czyz, *High Energy Particle Interactions with Nuclei*, in Proceedings, CERN School of Physics, Geneva 1978, pp. 1–20. A. Bialas, M. Bleszynski, and W. Czyz, *Nucl.Phys.* **B111**, 461 (1976). W. Czyz, *lectures on Theory of Hadron–Nucleus Scattering*, in Proceedings of International School of Nuclear Physics, Erice 1974, Amsterdam 1975, pp. 139–163.
- [2] P. Carruthers, *Annals of NY–Academy of Sciences*, Vol. 229, New York 1974, pp. 91–123.
- [3] R. Hagedorn and J. Rafelski, *Phys. Lett.* **97**, 180 (1980). J. Rafelski and R. Hagedorn, in: *Statistical Mechanics of Quarks and Hadrons*, H. Satz, ed., North Holland, (Amsterdam 1981) p. 253.
- [4] R. Hagedorn, *Suppl. Nuovo Cimento* **2**, 147 (1965). R. Hagedorn, *Cargèse lectures in Physics*, Vol. 6, Gordon and Breach (New York 1977) and references therein. R. Hagedorn and J. Rafelski in: *Statistical Mechanics of Quarks and Hadrons*, H. Satz, ed., North Holland, (Amsterdam 1981)

- p. 237. see also contributions in: J. Letessier, H. Gutbrod and J. Rafelski, *Hot Hadronic Matter*, Plenum Press NATO-ASI series B346 (New York 1995).
- [5] C. DeTar, *Quark Gluon Plasma in Numerical Simulations of lattice QCD*, in *Quark Gluon Plasma 2*, p. 1, R. Hwa, ed., World Scientific (Singapore 1995).
- [6] G. Baym, *Acta Phys. Pol. B*, this volume.
- [7] J. Rafelski, J. Letessier and A. Tounsi, *Acta Phys. Pol. B27*, 1035 (1996).
- [8] J. Rafelski, J. Letessier and A. Tounsi, *XXVI International Conference on High Energy Physics*, Dallas 1992, AIP-Conference Proceedings No 272, J.R. Sanford, ed., p.272. J. Letessier, A. Tounsi, U. Heinz, J. Sollfrank and J. Rafelski, *Phys. Rev. Lett.* **70**, 3530 (1993). M. Gaździcki, *Z. Physik C* **66**, 659 (1995).
- [9] J. Rafelski, *Phys. Rep.* **88**, 331 (1982).
- [10] P. Koch, B. Müller, and J. Rafelski, *Phys. Rep.* **142**, 167 (1986); *Z. Phys.* **A324**, 453 (1986).
- [11] T. Alber *et al.*, NA35 collaboration, *Phys. Lett B366*, 56 (1996).
- [12] J. Letessier, J. Rafelski and A. Tounsi, *Strangeness in Pb-Pb Collisions at 158A GeV*, *Phys. Lett. B*, in press, 1997.
- [13] I. Králik, WA97 Collaboration, CERN presentation May 12/13, 1997, *Hyperon and Anti hyperon Production in Pb-Pb Collisions at 158A GeV/c*, in [32].
- [14] Ch. Bormann, NA49 Collaboration, *Kaon,  $\Lambda$ , and  $\bar{\Lambda}$ -Production in Pb+Pb Collisions at 158 GeV per Nucleon*, IKF-Frankfurt report, May 1997, in [32].
- [15] G. Odyniec, NA49 Collaboration,  *$\Xi(\Omega)$  Production in Pb+Pb Collisions at 158 GeV/c*, Preprint LBL-40422, June 1997, in [32].
- [16] D. Evans, WA85 collaboration, p. 79 in [33]. M. Venables, WA94 collaboration, p. 91 in [33].
- [17] I.G. Bearden *et al.*, NA44 Collaboration, *Phys. Lett. B388*, 388 (1996). I.G. Bearden *et al.*, NA44 Collaboration, *Phys. Rev. Lett.* **78**, 2080 (1997).
- [18] J. Eschke NA35 collaboration, p. 105 in [33].
- [19] V. Friese, NA49 Collaboration,  *$\Phi$  production in 158 GeV/u Pb+Pb collisions*, IKF-Frankfurt report, May 1997, in [32]. and H. Ströbele and M. Gaździcki, private communication.
- [20] S. Abatzis *et al.*, WA85 Collaboration, *Phys. Lett. B* **376**, 251 (1996).
- [21] J. Letessier, J. Rafelski, and A. Tounsi, *Phys. Lett. B389*, 586 (1996).
- [22] L.R. Surguladze and M.A. Samuel, *Rev. Mod. Phys.* **68**, 259 (1996).
- [23] M. Schmelling, *Status of the Strong Coupling Constant*, in proceedings of ICHEP 1996, World Scientific, Singapore 1997, Z. Ajduk and A.K. Wróblewski, eds., p. 91.
- [24] T. Biró and J. Zimányi, *Phys. Lett. B113*, 6 (1982); *Nucl. Phys. A395*, 525 (1983). J. Rafelski and B. Müller, *Phys. Rev. Lett.* **48**, 1066 (1982); **56**, 2334E (1986).

- [25] J. Letessier, J. Rafelski and A. Tounsi, *Phys. Lett.* **B321**, 394 (1994); **B323**, 393 (1994); **B333**, 484 (1994); **B390**, 363 (1997).
- [26] J. Letessier, A. Tounsi, U. Heinz, J. Sollfrank and J. Rafelski, *Phys. Rev.* **D51**, 3408 (1995).
- [27] E. Shuryak and V. Thorsson, *Nuc. Phys.* **B536**, 739 (1992).
- [28] C. Gong, *J. Phys. G: Nucl. Part. Phys.* **18**, L123 (1992).
- [29] J. Sollfrank, M. Gaździcki, U. Heinz and J. Rafelski, *Z. Physik* **C61**, 659 (1994).
- [30] F. Fleuret, *Recherche du plasma de quarks et de gluons par l'étude des méson  $J/\Psi$  et  $\Psi'$  dans les collisions d'ions Plomb et de Protons ultra-relativistes sur divers noyaux*, Doctorat de l'Ecole Polytechnique, LPNHE-X, April 1997.
- [31] M. Gonin, NA49 Collaboration, in proceedings of QM'96, *Nucl. Phys.* **A395**, 525 (1983).
- [32] A.D. Panagiotou *et al.*, Proceedings of SQM'97 meeting, Thera, Greece, April 1997.
- [33] *Strangeness in Hadronic Matter*, Budapest 1996, T. Csörgö, P. Lévai and J. Zimányi, eds., *APHN N.S., Heavy Ion Physics* **4**, (1996), Akadémiai Kiadó, Budapest.